Multiphase methane-rich fluid inclusions in gold-bearing quartz as illustrated at Pontal (Goias, Brazil)

N. GUILHAUMOU[1], M. SANTOS[2], J. C. TOURAY[3], C. BENY[4], AND M. DARDENNE[2]

[1]Département de Géologie de l'Ecole Normale Supérieure, URA CNRS n° 1316, 24 rue Lhomond, 75005 Paris, France

[2]Instituto de Geociencias, Universidad de Brasilia, Brasilia, Brazil

[3]Laboratoire de Métallogénie et Géochimie minérale, Ecole Supérieure de l'Energie et des Matériaux, URA CNRS n° 1366, Université d'Orléans, 45067, Orléans Cédex 02, France

[4]G.S. (BRGM-CNRS), 1A, rue de la Férollerie 45071, Orléans Cédex 02, France

Abstract

In the Pontal auriferous lode, dominant saccharoidal quartz is associated with oligoclase, biotite, hornblende, tremolite–actinolite, sulphides (less than 2%), and disseminated native gold. Four main types of fluid inclusion have been distinguished based on their habit, distribution and spatial relationship with gold particles. Type S are primary multiphase large sized (100 to 200 μm) inclusions with homogenization temperatures ($V + L \rightarrow L$) between 350 and 450 °C. They contain siderite and/or calcite and graphite-like microcrystals as daughter phases. Commonly associated with these inclusions are tiny (50 to 100 μm) solid inclusions of biotite or actinolite. In most of these inclusions, only CH_4 has been detected in the vapour phase. However some noticeable exceptions were observed (CO_2/CH_4 ratio near 0.85). Type C inclusions are later than gold and occur disseminated in quartz or along trails that crosscut quartz grain boundaries. They may contain nahcolite daughter crystals. CO_2/CH_4 ratios range from 0.0 to 0.5. Homogenization temperatures vary from 150 to 300 °C. Type V are mainly gaseous CH_4–H_2O inclusions. They may occur as small-sized inclusions directly associated with gold particles. Type L are aqueous two-phase inclusions of late secondary origin.

The scattering of the CO_2/CH_4 ratios could be related to fluctuations of the oxygen fugacity that triggered gold precipitation at the time of trapping. These variations of f_{O_2} with time could reflect unbuffered fluid–rock interaction with respect to redox conditions during quartz deposition.

Finally, gold deposition is interpreted to have occurred at elevated temperature (500 °C) and pressure, compatible with boundary conditions between greenschist and amphibolites facies.

KEYWORDS: gold deposit, quartz lode, fluid inclusions, Raman microprobe, microthermometry.

Introduction

A COMPOSITE depositional model for lode gold deposits (Colvine *et al.*, 1988) shows an evolution from upper-level deposits, where brittle deformation predominates, to lower ones with dominant ductile deformation. Data are available from fluid inclusions in upper level deposits that illustrate the rôle of H_2O–CO_2 fluids and the irregular occurrence of elevated CH_4 contents (see e.g. Colvine *et al.*, 1988; Touray *et al.*, 1989). On the other hand, little is known about fluid inclusions in deep-seated deposits that formed at the onset of retrograde processes, after metamorphic culmination.

In this paper we describe such inclusions in an auriferous quartz lode, conformable with the foliation of host mylonitic gneisses and associated with a limited actinolite + biotite alteration halo.

Regional geology, ore geology and mineralogy

The Pontal mine (Brejinho de Nazaré) is located in the NE part of the former Goias State, now the Tocantins State, about 400 km north of Brasilia (Fig. 1). Presently, 10^4 tons of gold-bearing quartz (average grade 17.5 ppm gold) have been mined by METAGO from a lens 120 m long, 0.50 m thick and 60 to 100 m deep. Other similar prospects are known in the area.

Mineralogical Magazine, June 1990, Vol. 54, pp. 257–266

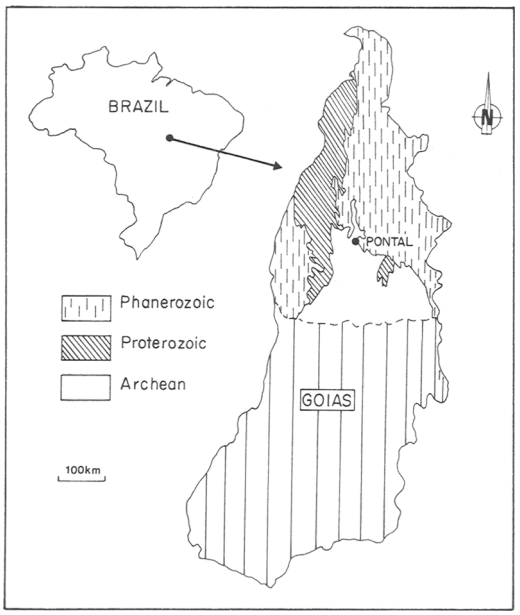

FIG. 1. Localization of the Pontal deposit (Tocantins state, Brazil).

Rocks exposed in the mine area consist of biotite and biotite–hornblende orthogneisses derived from tonalites, with amphibolite intercalations (Santos, 1989). The observed mineral associations are diagnostic of metamorphic culmination in the amphibolite facies; the lack of index minerals such as cordierite or sillimanite precludes any more precise conclusion. The orthogneisses display a mylonitic foliation orientated 015° to 030° and dipping 60° to 70°SE. A subhorizontal stretching lineation is defined by orientated biotite platelets; the various aspects of planar and linear deformation suggest a transcurrent ductile deformation in a dextral simple shear regime (Santos, 1989).

Auriferous quartz lodes, including the one mined, are usually parallel to the mylonitic foliation and sometimes cut it at a low angle; quartz lodes are deformed by boudinage, with deformation axes nearly parallel to the stretching lineation present in the orthogneisses. Segregation of auriferous quartz before the end of ductile deformation of the host rock is assumed (Santos, 1989).

Later granitic intrusions containing xenoliths of mylonitic orthogneiss have been dated at 1737 ± 50 Ma (Costa and Hasui, 1989). Related to these intrusions are pegmatitic injections that cut both metamorphic basement and auriferous quartz lodes. North of the mine area, the Precambrian basement is unconformably overlain by Devonian detrital sediments (Pimenteiras Formation).

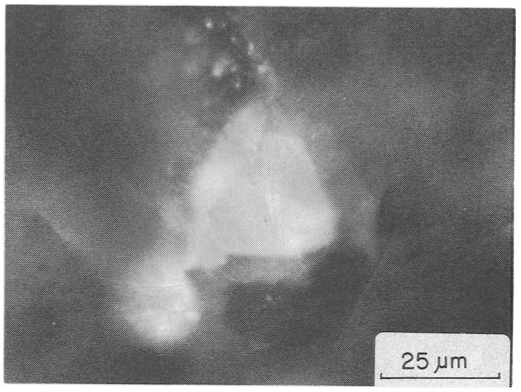

FIG. 2. Photomicrograph of a euhedral gold crystal.

In conclusion, the auriferous quartz lode mined at Pontal formed before 1.7 Ga and presumably during early Proterozoïc times; this process occurred after metamorphic culmination of the host basement in the amphibolite facies, but ductile deformation was still occurring. A petrological interpretation of the mineral association trapped in quartz as solid inclusions as well as a study of its fluid inclusions were necessary to define the physico-chemical conditions prevailing during ore deposition. At the top and base of the quartz lens, the host gneiss is marked by a dark zone with notable enrichment in biotite and actinolite. This high-T and P alteration of the host rocks is significant for the paragenesis of the lode deposit.

Solid inclusions in auriferous quartz

The auriferous lode is composed dominantly of white to grey saccharoidal quartz showing undulose extinction, with indentated and sutured contacts. Other components associated with quartz are gold, different silicates and around 2% of sulphides (pyrrhotite, pyrite, chalcopyrite and rare galena and sphalerite).

Native gold is disseminated in the quartz lens as irregular and euhedral crystals (Fig. 2), with sizes spanning from 0.02 to 0.6 mm. More rarely, gold filling fractures was noticed. Microscopic investigations of quartz revealed solid inclusions of amphibole, feldspar and mica. Raman spectroscopy of these amphiboles gave spectra essentially identical to a reference actinolite (communicated by J. M. Beny). For feldspar, the recorded Raman spectrum is characteristic of a sodic plagioclase.

	n° 5	n° 19	n° 16	n° 14	n° 17	n° 18	n° 28	n° 36
SiO_2	36.94	37.26	36.03	51.96	50.16	59.31	60.94	58.15
TiO_2	2.42	3.11	3.25	0.65	0.48	0.O	0.0	0.0
Al_2O_3	16.05	15.40	14.56	8.32	5.08	24.96	24.15	25.60
FeO*	18.31	17.15	19.84	12.86	13.83	0.0	0.0	0.0
MnO	0.21	0.26	0.21	0.18	0.38	0.0	0.0	0.0
MgO	10.65	11.32	10.10	10.32	13.25	0.0	0.0	0.0
CaO	0.10	0.21	0.0	10.65	11.95	6.45	5.63	7.34
Na_2O	0.14	0.28	0.06	0.78	0.47	7.58	8.50	7.33
K_2O	9.19	9.32	9.75	0.48	0.36	0.05	0.11	0.07
H_2O	3.87	3.72	3.84	1.97	1.98	0.0	0.0	0.0
Total	97.88	93.03	97.64	98.17	97.94	98.35	99.33	98.49
Phases		biotites		amphiboles			plagioclases	

TABLE 1. Chemical composition of trapped minerals in quartz. Electron microprobe data; nos. 5, 16, 19 = biotites; nos. 14, 17 = amphiboles; nos. 18, 28, 36 = plagioclases.

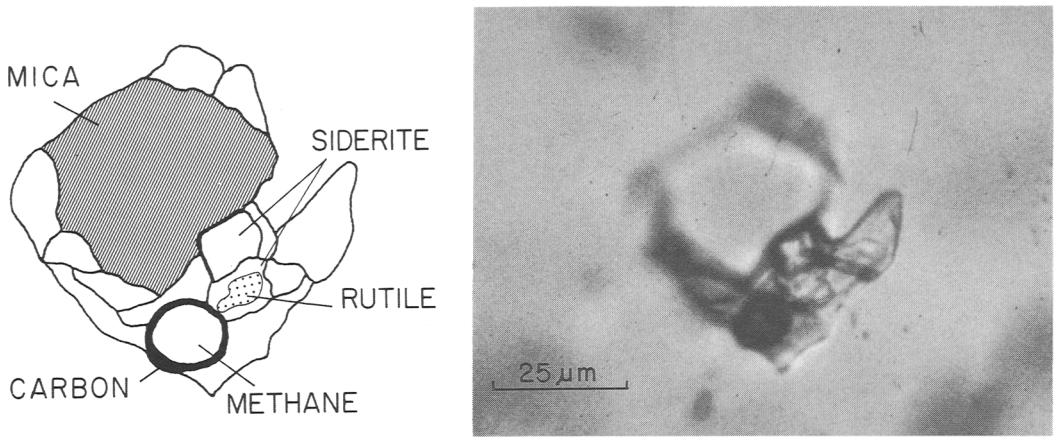

FIG. 3. Sketch and photomicrograph of an S-type inclusion with trapped biotite crystals and several other solids.

About 50 electron microprobe analyses of trapped minerals within quartz have been carried out. Because of contamination by enclosing quartz or other associated phases, only a limited number of these have been selected for discussion (Table 1). Biotite is very similar to dark brown biotite described in the literature (Deer *et al.*, 1973, p. 62; table 13 no. 2). Amphiboles belong to the calcic group and may be classified as actinolites near the boundary with actinolitic hornblende. Plagioclase ranges in composition from Ab_{72} to Ab_{64}, not far from oligoclase-andesine.

Fluid-inclusion studies

Typology. Four main types of fluid inclusion have been defined from microscopical observations:

1. S-type are large (about 100 µm) multiphase primary (vapour/liquid) inclusions, with a low degree of filling (0.1 to 0.2). They are isolated within quartz grains and contain several solids with distinct shape, colour, refractive index and birefringence (Fig. 3). Amongst these solids, large trapped mineral grains were probably responsible

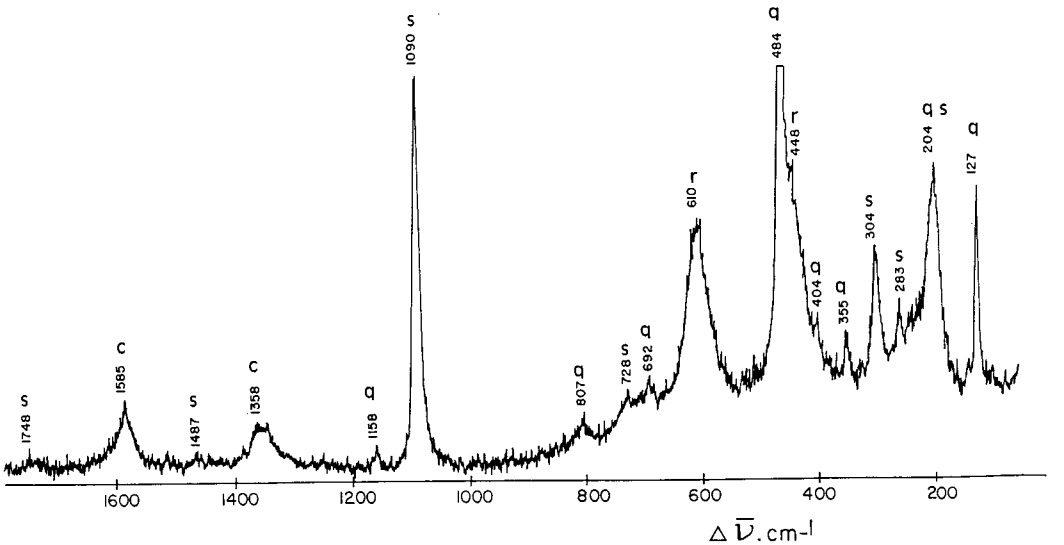

FIG. 4. Raman spectrum of an aggregate of solid phases within a S-type inclusion. q = quartz from matrix, r = rutile, c = carbon, s = siderite.

for the formation of S-inclusions; they are brown platelets (recognized to be biotite) and greenish pleochroic blebs with noticeable birefringence, very similar to the actinolite inclusions present in the quartz matrix.

2. C-type are medium-sized (about 20 to 40 μm) pseudo-secondary and/or secondary inclusions; they form groups within a same crystal or trails cross-cutting boundaries of quartz grains. They contain (L + V) or (L + V + S) phase assemblages, with a degree of filling of about 0.3 to 0.4; liquid CO_2 has sometimes been observed at room temperature.

3. V-type are small to medium sized inclusions with a degree of filling of about 0.9; they appear scattered within the quartz crystals, sometimes in a geometrical relationship with gold grains; their relative age and their spatial relations with S and C types have not been clearly established.

4. L-type are aqueous two-phase inclusions of late secondary origin.

Raman microprobe data. Raman spectra of gas and solids in S, C and V inclusions have been obtained using a U 1000 apparatus. Analytical conditions have been described elsewhere (Touray *et al.*, 1988). Examples of Raman spectra for solid phases are given in Figs. 4 and 5; results are summarized in Table 2.

S-type inclusions contain trapped biotite and amphibole which gave poorly-defined Raman spectra, although comparable with spectra from the same phases trapped as isolated large inclusions in the quartz matrix. Rutile, with characteristic peaks occurring at 448 and 610 cm^{-1} was detected in S inclusions. Other solids form smaller grains apparently not present as solid inclusions in quartz. They could be daughter phases, although they are only slightly soluble on heating. These later phases were determined as:

Graphite-like grains. Poorly ordered carbon was identified by two broad bands at about 1360 and 1590 cm^{-1}, corresponding to undulated and zig-zag textures (Rouzaud, 1984).

Rhombohedral carbonates. Two or three crystals may be present simultaneously. From reference Raman spectra these carbonates are siderite, or more rarely, dolomite, and/or calcite, as shown by characteristic peaks on Raman spectra (Table 3).

In the vapour phase, only CH_4 has been detected in most of the S inclusions, with some noticeable exceptions (Table 2). On the other hand, the detection limit of CO_2 in such inclusions is probably in the range 5–10 mole percent, when one refers to the signal to noise ratio. Accordingly, 'pure' CH_4 inclusions, as indicated in Table 2, may well contain several percent of CO_2 and/or N_2.

C-type inclusions may host one or several daughter crystals of nahcolite (Fig. 5). The gas phase usually contains higher CO_2 and lower CH_4 amounts than the S inclusions; nitrogen has rarely been detected (Table 2). In V-type inclusions only

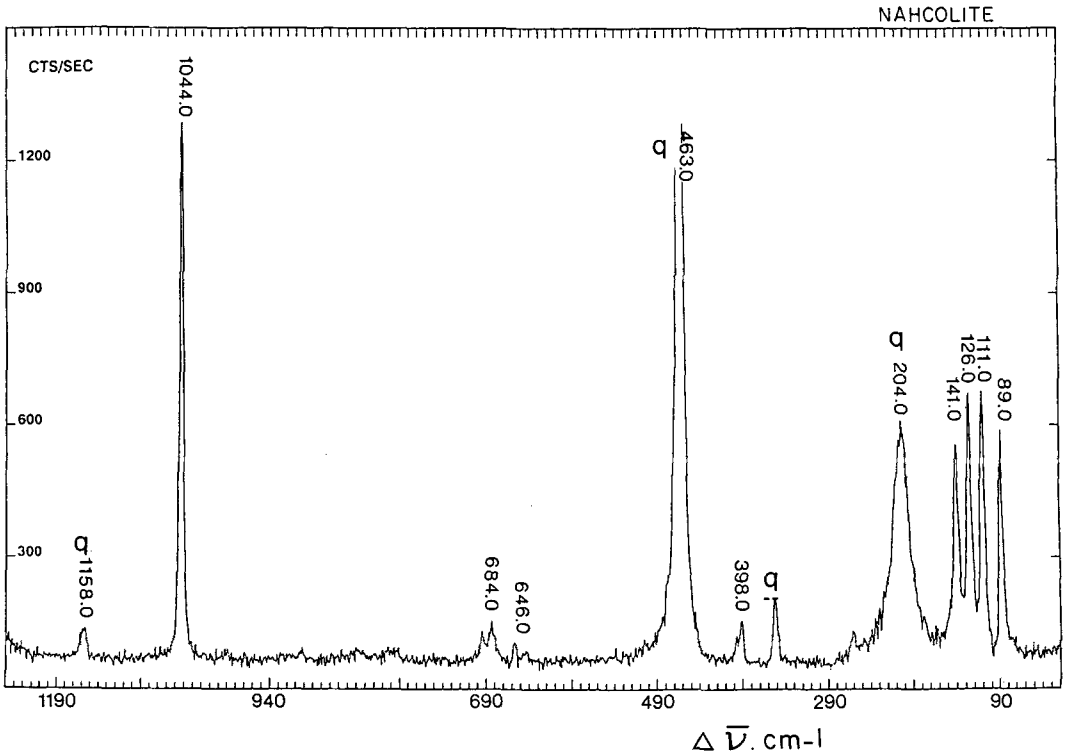

FIG. 5. Raman spectrum of nahcolite within a type C inclusion. q = quartz from matrix.

CH_4 and sometimes nitrogen have been detected (Table 2). L type inclusions do not contain any detectable volatiles.

Microthermometric data. In S-type inclusions, phase transitions at low temperature are extremely difficult to observe. During freezing runs, phase transitions were looked for, but were not observed in S inclusions without detectable CO_2; only inclusions 1A1S00 and 2AS00, containing dominant CO_2 (Table 2), displayed a visible $L + V \rightarrow L$ transition at $-6\,°C$, but solid CO_2 was not observed. At high temperatures, homogenization of the fluid phases was from 280 to 450 °C in the liquid phase (Fig. 8). Some dissolution of the carbonates (possible daughter minerals) was observed during several heating runs.

In V-type inclusions, only homogenizations into the vapour phase were observed (360 to 460 °C). In C-type inclusions, freezing experiments yielded the following data: the melting temperature of CO_2 (Fig. 6) varied from -56.6 to about $-70\,°C$; similarly, the homogenization temperatures of the CO_2 phases were extremely variable (Fig. 7). These data are in good agreement with the large range of CO_2/CH_4 ratios determined by Raman microspectrometry (Table 2).

A noticeable scattering of the clathrate melting temperature (+6 to +18 °C), usually above the value for pure CO_2 (+10 °C, according to Hollister and Burruss, 1976), is compatible with the presence of variable CH_4 amounts (Collins, 1979). The last melting of ice, determined in the presence of clathrate, occurred between $-2\,°C$ and $-4\,°C$, indicative of dilute aqueous solutions. Homogenization temperatures scatter in the 250–300 °C range. Dissolution of nahcolite (daughter mineral) was observed around 180 °C.

L-type inclusions displayed last melting temperatures of ice in the $-2\,°C$ to $-5\,°C$ range (dilute solutions); homogenization occurred on heating in the liquid phase, between 160 and 250 °C.

Interpretations and conclusions

In the gold-bearing quartz lode mined at Pontal, the formation of S-type fluid inclusions is synchronous with the trapping of oligoclase, acti-

REFERENCE	TYPE	RAMAN ANALYSIS								OBSERVATIONS
		SOLID PHASES				GASEOUS PHASES				
		Fe Carbonates	Graphite like	Rutile	Nahcolite	CO_2	CH_4	N_2	CO_2/CH_4	
N 35 110										
1 A 1 S 00	S	+	+	+	–	81	19	–	4.26	Amphibole
2 A S 00	S	+	+	+	–	82	18	–	4.55	"
110 A S 00	S	nd	nd	nd	–	–	100	–	–	Biotite
INCA	S	+	+	+	–	–	100	–		"
110 X 1	S	+	–	–	–	–	100	–		"
2 E S 00	C	–	–	–	+	–	100	–		
2 B S 00	C	–	–	–	+	–	100			
2 C S 00	C	–	–	–	+	–	100	–		
2 D S 00	C	–	–	–	+	–	100			
110 A S 00	C	–	–	–	nd	–	100	–		
M 10 A	V	–	–	–	–	–	100	–		Around Au particles
M 10 B	V	–	–	–	–	–	100	–		"
N 3580 B										
85 M S 00	S	+	+	+	–	–	100			Biotite
85 A S 00	S	+	+	+	–	–	100	–		"
35 D S 00	S	+	–	+	–	–	100	–		"
35 A S 00	S	+	+	+	–	–	100	–		"
85 E	V	–	–	–	–	–	99	1	–	Around Au particles
85 F	V	–	–	–	–	–	100	–	–	"
86 G	V	–	–	–	–	–	100	–	–	"
85 H	V	–	–	–	–	–	99	1	–	"
85 J	V	–	–	–	–	–	100	–	–	"
85 I	V	–	–	–	–	–	90	10	–	"
85 K	V	–	–	–	–	–	99	1	–	"
N 15										
8 CA S 00	S	+	+	+	–	–	100	–	–	+ $CaCO_3$
8 CC S 00	C	–	–	–	+	–	100	–	–	
N 22										
22 1 B S 00	C	–	–	–	–	86	14	–	6.14	
22 1 A S 00	C	–	–	–	–	98	2	–	49	
22 B d S 00	C	–	–	–	+	89	11	–	8.1	
22 B a S 00	C	–	–	–	–	94	6	–	15.6	
22 T a S 00	C	–	–	–	–	95	5	–	19	
22 B B S 00	C	–	–	–	–	15	58	27	0.26	
22 A A S 00	C	–	–	–	–	84	16	–	5.25	
B C S 00	C	–	–	–	+	–	100	–	–	
B B S 00	C	–	–	–	+	18	82	–	0.22	
B E S 00	C	–	–	–	+	16	84	–	0.19	
B C S 00	C	–	–	–	+	–	100	–	–	

TABLE 2. Interpretation of the Raman microprobe data for fluid inclusion contents. Reference = reference of the spectrum. nd = solid phase observed but not accurately determined. — = not observed for solid phases and undetected for gaseous phases analyses. Proportions as mole %.

nolite, biotite and native gold (solid inclusions in quartz). S-inclusions are hence of primary origin. In addition to biotite, rutile, and actinolite, S-type inclusions contain graphite and ferriferous carbonates. The question arises whether these last phases, not observed as solid inclusions in quartz, are trapped or daughter minerals. Unfortunately, no straightforward answer can be given: graphite particles may have precipitated *in situ* or have been transposed in suspension; only carbonates,

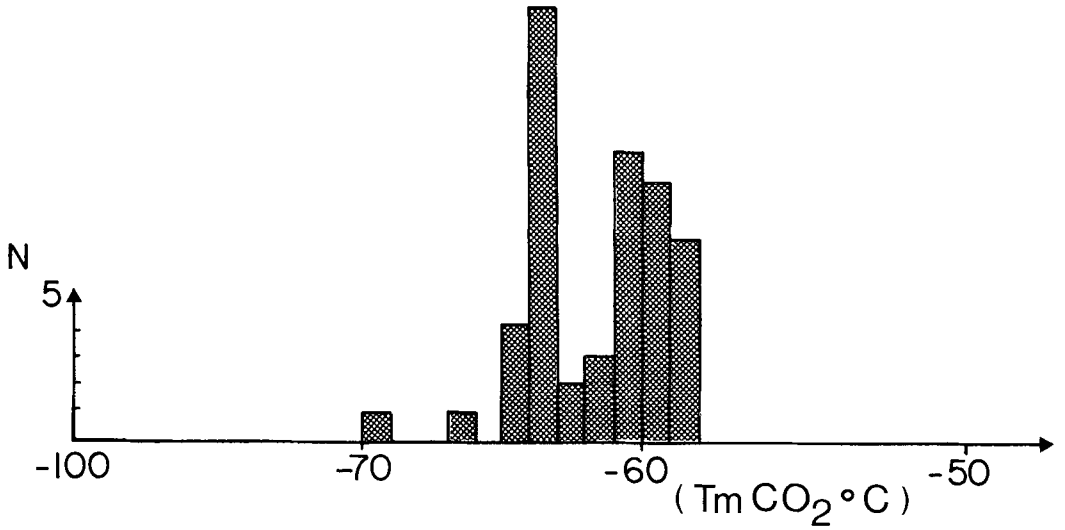

FIG. 6. Histogram of the melting temperature Tm of CO_2 in type C inclusions.

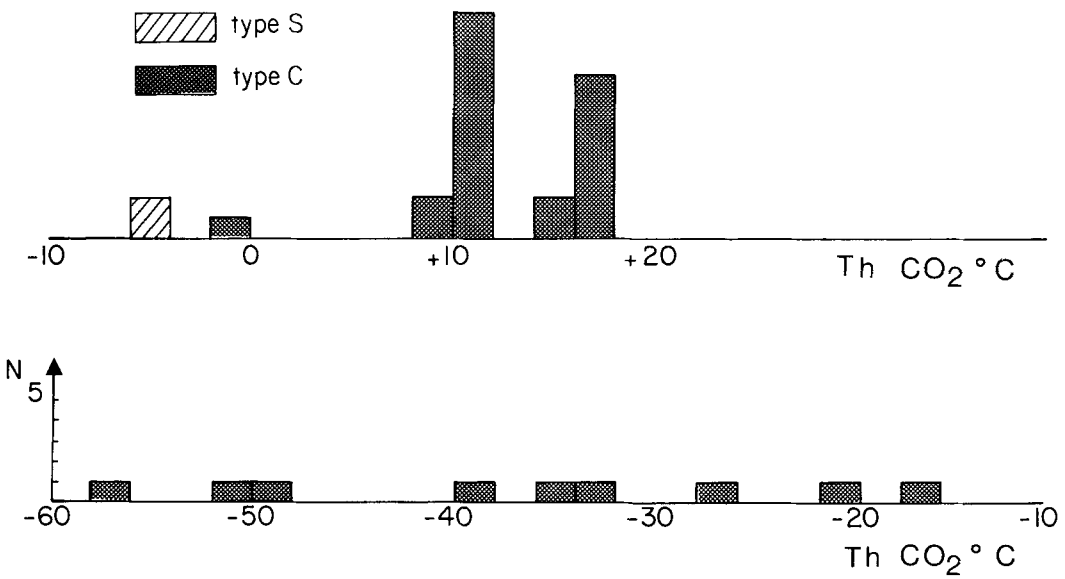

FIG. 7. Histogram of the homogenization temperatures of the CO_2 phases (L + V → L) in type C and S inclusions.

whose limited dissolution has been sometimes noticed, were at least *pro parte* deposited as daughter phases.

Most of the S-type inclusions contain only detectable methane as a volatile component, but some inclusions (Table 2) are dominated by CO_2. At 500 °C, with $f_{CO_2}/f_{CH_4} = 4$ and equilibrium with graphite, f_{O_2} plots on the QFM buffer or slightly higher or lower, depending on pressure (Kreulen, 1987, FIg. 1). For inclusions without detectable CO_2, f_{O_2} is evidently lower but cannot be estimated. These results may be compared with the data obtained from the Sanoukou prospect (Touray, 1987) indicating, in the 300–350 °C range, redox conditions near the Ni–NiO buffer. Bearing in mind possible variations of the CO_2/

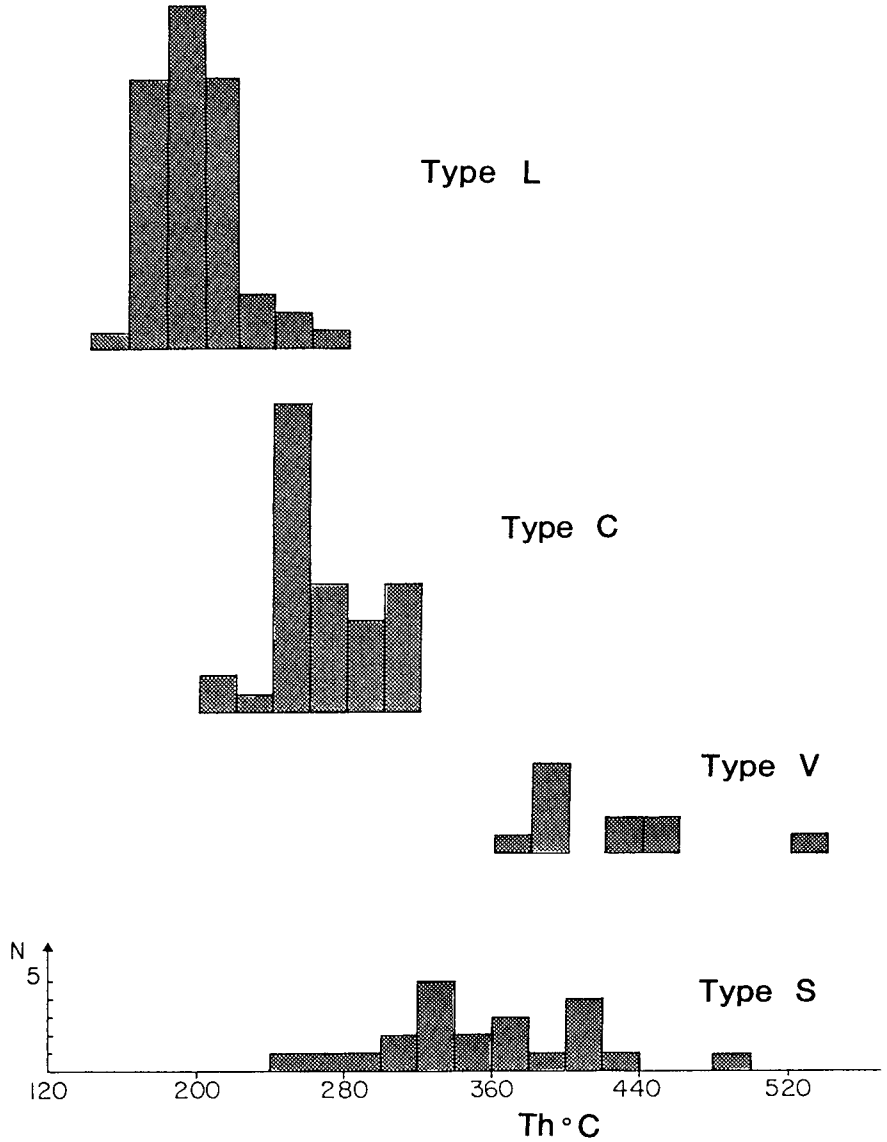

FIG. 8. Histograms of the total homogenization temperatures of the different inclusions types.

CH_4 ratio resulting from the precipitation of the graphitic phase (Dubessy, 1984), such a scattering may illustrate actual variations of the initial CO_2/CH_4 ratio and hence fluctuations of the oxygen fugacity at the time of trapping.

Variable f_{O_2} through time could reflect unbuffered fluid–rock interactions with respect to redox conditions at the site of quartz deposition. Variations of f_{O_2} may have triggered gold precipitation through destabilization of $Au(HS)_2^-$ complexes after variation of the oxygen fugacity (Touray, 1987; Shenberger and Barnes, 1989).

C-type inclusions represent early circulation of secondary fluids with variable CO_2/CH_4 ratios (Table 2). L-inclusions correspond to late hydrothermal aqueous solutions. The origin and age of V-inclusions are not clear; they represent high-temperature and low-density methane-rich fluids

Référence		$2\nu_2$	νCO_3	ν_4	L	T	
N35110							
IFC	S_1	1753	1094	722	295	170	Dolomite
	S_2	1737	1091	733	300	~ 192	Sidérite
IFA	S_1	1736	1089	735	302	~ 196	Sidérite
A35	S_1	–	1092	734	305	200	Sidérite
N3580B							
IFD	S_1	–	1090	736	304	~ 195	Sidérite
IFA	S_1	–	1092	730	306	197	Sidérite
A35α	S_1	1744	1091	735	310	~ 193	Sidérite
IA	S_1	–	1092	736	306	193	Sidérite
N15							
8CA	S_1	–	1094	723	299	171	Calcite – dolomite
	S_2	–	1087	713	283	156	Calcite

TABLE 3. Raman microprobe data for carbonates in type S inclusions. Reference = inclusion reference; $2\nu_2$ = out of plane bend; νCO_3 = symmetric stretch of CO in CO_3; ν_4 = in plane bend; T = translation mode; L = libration mode. From Bischoof *et al.* (1985). — = peak position not accurately determined.

and are sometimes geometrically related to gold particles. No convincing evidence supports the hypothesis of coeval S and V-type inclusions.

Homogenization temperatures indicate a trapping of S type inclusions (and hence of gold particles) above 280 to 450 °C, provided that the highest T_h did not result from stretching (e.g. at the time of injection of the pegmatitic dykes). From petrographic arguments, the trapping of the S-type multiphase and of the solid inclusions in quartz (including gold), occurred under the T–P conditions prevailing at the boundary between the greenschist and the amphibolite facies (biotite + actinolite + oligoclase stable). Referring to several authorities (Winkler, 1974; Turner and Verhoogen, 1958), *T* may be estimated to about 500–550 °C, *P* being more difficult to constrain.

Finally, the Pontal gold-bearing quartz vein may be described as a high-temperature metamorphic deposit (Moravek and Pouba, 1987), probably formed under variable oxygen fugacity, with redox conditions ranging from QFM buffer to lower values. A major unresolved problem is the origin of the carbon-bearing fluids: the usual assumption of a source within graphitic shales cannot be invoked, in view of the lack of such sediments in the basement. Some deep crustal (or mantle?) source appears more probable.

Similarly, the classical hypothesis of a gold source within local ultrabasic rocks seems unlikely, and some deep source has to be invoked.

Acknowledgements

The authors acknowledge the CAPES-COFECUB and the PIRSEM-CNRS for financial support. Two anonymous referees and D. Jones helped to improve an earlier draft of this article.

References

Bischoft, W. D., Sharma, S. K. and Mackenzie, F. T. (1985) Carbonate ion disorder in synthetic and biogenic magnesium calcites: a Raman spectral study. *Am. Mineral.* **70**, 581–9.

Collins, P. J. L. (1979) Gas hydrates in CO_2-bearing fluid inclusions and the use of freezing data for estimation of salinity. *Econ. Geol.* **74**, 1435–44.

Colvine, A. C., Fyon, J. A., Heather, K. B., Soussan Marmont, Smith, P. M. and Troop, D. G. (1988) Archean lode gold deposits in Ontario. *Ontario Geol. Surv. Misc. Pap.* **139**, 136 pp.

Deer, W. A., Howie, R. A. and Zussman, J. (1963) *Rock forming minerals*, **3** (*Sheet-silicates*), 263 pp. Longmans, London.

Dubessy, J. (1984) Simulation des équilibres chimiques dans le système C–OH. Conséquences méthodologiques pour les inclusions fluides. *Bull. Minéral.* **107**, 155–68.

Hollister, L. S. and Burruss, R. C. (1976) Phase equilibria in fluid inclusions from the Khtada Lake metamorphic complex. *Geochim. Cosmochim. Acta*, **40**, 163–75.

Kreulen, R. (1987) Thermodynamic calculations of the C–O–H system applied to fluid inclusion: are fluid inclusions unbiassed samples of ancient fluids? *Chem. Geol.* **61**, 59–64.

Moravek, P. and Pouba, Z. (1987) Precambrain and Phanerozoic History of Gold Mineralization in the Bohemian Massif. *Econ. Geol.* **82**, 2098–114.

Rouzaud, J. N. (1984) Thèse de doctorat d'Etat, Université d'Orléans, 139 pp.

Santos, M. (1989) Mestrado thesis, University of Brasilia, 134 pp.

Shenberger, D. M. and Barnes, H. L. (1989) Solubility of gold in aqueous sulfide solutions from 150 °C to 350 °C. *Geochim. Cosmochim. Acta*, **53**, 269–78.

Touray, J. C. (1987) Transport et dépôt de l'or dans les fluides de la croûte continentale, l'apport des études d'inclusions fluides. *Chron. Rech. Minière*, **484**, 43–53.

——Beny, C., Bouhlel, S. (1988) Caractérisation, par analyse à la microsonde électronique et microspectrométrie Raman, de barytocélestites de différentes compositions. *C.R. Acad. Sc. Paris*, **306**, 1353–7.

——Marcoux, E., Hubert, P. and Proust, D. (1989) Hydrothermal Processes and Ore Forming Fluids in the Le Bourneix Gold Deposit, Central France. *Econ. Geol.* **84**, 326–37.

Turner, F. J. and Verhoogen, J. (1958) *Metamorphic reactions and metamorphic facies*. New-York, Geol. Soc. Amer., 259 pp.

Winkler, H. G. F. (1974) *Petrogenesis of metamorphic rocks*. Berlin, Heidelberg, Springer Verlag, 220 pp.

[*Manuscript received 28 June 1989; revised 15 January 1990*]